IEEE Access
Multidisciplinary | Rapid Review | Open Access Journal

Received June 14, 2019, accepted June 30, 2019, date of publication July 3, 2019, date of current version July 23, 2019.

Digital Object Identifier 10.1109/ACCESS.2019.2926497

An Active Learning Method for DEM Extraction From Airborne LiDAR Point Clouds

ZHENYANG HUI[1,2,3], SHUANGGEN JIN[2,4], (Member, IEEE), PENGGEN CHENG[1,3], YAO YEVENYO ZIGGAH[5], LEYANG WANG[1], YUQIAN WANG[1], HAIYING HU[1,3], AND YOUJIAN HU[6]

[1]Faculty of Geomatics, East China University of Technology, Nanchang 330013, China
[2]School of Remote Sensing and Geomatics Engineering, Nanjing University of Information Science and Technology, Nanjing 21044, China
[3]Key Laboratory for Digital Land and Resources of Jiangxi Province, East China University of Technology, Nanchang 330013, China
[4]Shanghai Astronomical Observatory, Chinese Academy of Sciences, Shanghai 200030, China
[5]Faculty of Mineral Resources Technology, University of Mines and Technology, Tarkwa 00233, Ghana
[6]Faculty of Information Engineering, China University of Geosciences, Wuhan 430074, China

Corresponding author: Penggen Cheng (pgcheng1964@163.com)

This work was supported in part by the National Natural Sciences Foundation of China under Grant 41801325, Grant 41861052, and Grant 41874001, in part by the Education Department of Jiangxi Province under Grant GJJ170449, in part by the Key Laboratory for Digital Land and Resources of Jiangxi Province, East China University of Technology, under Grant DLLJ201806, and in part by the East China University of Technology Ph.D. Project under Grant DHBK2017155.

ABSTRACT Airborne Light Detection and Ranging (LiDAR) is a popular active remote sensing technology that has been developing very rapidly in recent years. To solve the problems of low filtering accuracy of airborne LiDAR point clouds in complex terrain environments and avoiding too much human intervention, this paper proposes a point cloud filtering method based on active learning. In the proposed method, the initial training samples are acquired and marked automatically by multi-scale morphological operations. In so doing, no training samples are selected and labeled manually, i.e., the training samples are added gradually according to the oracle used in active learning. In this paper, the oracle is set to a sigmoid function of residuals from the points to the fitted surface. Subsequently, the training model is revised progressively using the updated training samples. Finally, the classification results are further optimized by a slope-based method. Three datasets with different filtering challenges provided by the International Society for Photogrammetry and Remote Sensing (ISPRS) were used to test the proposed method. Comparing with the other ten famous filtering methods, the proposed method can achieve the smallest average total error (5.51%). Thus, it can be concluded that the proposed method performs very well toward different terrain environments.

INDEX TERMS Active learning, airborne LiDAR, point cloud filtering, oracle, training sample.

I. INTRODUCTION

As an active remote sensing technology, airborne LiDAR has rapidly developed in recent years. Compared with traditional passive remote sensing methods, such as photogrammetric mapping, airborne LiDAR can acquire accurate three-dimensional point clouds data directly to characterize the topographic profile of the earth surface [1]. Moreover, LiDAR pulses can penetrate tree canopy to record the terrain details [2]. Thus, airborne LiDAR has been widely used for digital terrain model (DTM) generation [3], [4].

DTM generation is a crucial step in LiDAR point cloud data processing applications, such as road extraction [5], [6], object classification [7], [8], and forest parameter estimation [9], [10]. Therefore, lots of researchers have been involved in developing algorithms for DTM extraction from airborne LiDAR point clouds [3], [11], [12]. This process is commonly known as filtering. Nowadays, many famous filtering algorithms have been put forward. According to their filtering principles, these methods can be categorized into seven classes, namely slope-based, morphology-based, surface-based, triangular-irregular-network-based (TIN), segmentation-based, statistic-based and energy-optimization-based.

Vosselman [13] first proposed the slope-based approach. In the method, the points with slope changes greater than a predefined threshold are extracted as the non-ground points. Generally, this method performs well in gentle slope areas but

The associate editor coordinating the review of this manuscript and approving it for publication was Wei Liu.

cannot achieve satisfactory accuracy in complicated terrain environments. To solve this problem, some improved methods have been proposed to enhance the robustness of this kind of approach by making the slope thresholds adaptive to abrupt terrains [14], [15].

The morphology-based methods filter non-ground points using a series of morphological operators, such as opening, top-hat and morphological reconstruction [16]. The key for achieving a good filtering performance relies on choosing an appropriate structure element. To remove the objects with different sizes, Zhang *et al.* [17] proposed a filtering method with a progressive strategy and adaptive sizing of the structural element. Subsequently, many other modified morphological filtering methods have been developed based on this pioneering work to improve filtering accuracy and protect terrain details [18]–[21]. However, most of these morphological filters need to predefine the largest size of the structure element. Aiming to free the limitation of structure element, Li *et al.* [1] proposed a novel morphological filter based on geodesic transformations of mathematical morphology. Hui *et al.* [2] applied a series of morphological top-hat operations to detect the optimal maximum filtering window automatically. Both of these two methods can enhance the robustness and automation of the morphological filters for unknown terrain environments.

The surface-based approaches realize filtering by means of certain interpolation methods [4], [22]. Kraus and Pfeifer [23] first generated a surface and then updated it iteratively with appropriate selection of ground points. Mongus and alik [24] developed a parameter-free algorithm using a Thin Plate Spline (TPS) interpolator, which was quickly improved by Chen *et al.* [25] who proposed a multi-resolution hierarchical classification (MHC) algorithm. Hu *et al.* [26] also adopted TPS to interpolate a raster surface. However, in their method bending energy was calculated as a byproduct of TPS interpolation, which can be used to calculated adaptive threshold automatically.

The TIN-based methods are similar to the surface-based methods. In contrast, the rough surface for the TIN-based methods is generated by building triangular irregular network. Axelsson [27] first proposed a progressive TIN densification (PTD) filtering method, which has been applied in commercial software named TerraScan. Although PTD has been proven to be the most effective algorithm in the experiments tested by Sithole and Vosselman [28], there are still some unresolved problems, such as deficiencies in dealing with discontinuities (edges, steep hills, etc.) and inability to filtering out attached objects (bridge, ramp, etc.). To improve the filtering accuracy at discontinuities, Zhang and Lin [29] embedded smoothness-constrained segmentation, whereas Zhao *et al.* [30] used morphological opening operation to obtain more potential ground seeds.

The segmentation-based approaches have been proved to perform better than some other methods such as the surface-based method and the PTD method, since the segmented results can provide additional geometric, texture and other features [31]–[33]. Nevertheless, these methods cannot achieve satisfactory filtering results in forested areas as little laser pulses can pretreat tree crowns to reach ground. Moreover, the filtering performance deeply depends on the segmentation accuracy [3].

The realization of statistic-based approaches is based on two assumptions. On one hand, the LiDAR ground points are assumed to be normally distributed under natural conditions. However, the non-ground points disturb the normal distribution and make it to be a positive skewness distribution. The basic idea of this kind of approaches is to keep removing object points until the skewness is balanced [34]. Bartels *et al.* [35] first developed this unsupervised algorithm called skewness balancing, which was quickly improved by Bao *et al.* [36] to address more complicated scenes. Bao *et al.* [37] further developed the statistical approach incorporating with the measure of kurtosis, and applied the modified algorithm to LiDAR intensity information to separate ground points and vegetation points in wooded areas. Bartels and Wei [38] extended the skewness balancing algorithm to make it adapt to sloped terrains.

Elmqvist [39] first proposed an energy-optimization-based filtering algorithm in form of active shape model. Energy of the model is a weighted combination of internal force and external force. The minimization of the energy function is processed iteratively until the step size of the model is less than a threshold. Hu *et al.* [40] developed a semi-global filtering (SGF) algorithm by defining a novel energy function that is composed of a data term and a regularization term. Ural and Shan [41] presented a Min-cut Based Filtering (MBF) algorithm on the basis of an energy function, which considers both local and global features. To minimize the energy function, a minimum cut optimization algorithm was applied. The test reveals that an overall filtering accuracy of 91.3% can be achieved for the ISPRS test areas. Similarly, He *et al.* [16] also extracted ground points progressively through energy minimization using graph cuts. In this method, the energy function and graph model encode both point-wise closeness and pairwise smoothness.

Although the above-mentioned methods perform well in most terrain environments, most of them need to adjust several parameters to achieve satisfactory filtering accuracy. To reduce parameter settings, some researchers try to apply machine learning or deep learning for filtering. Lu *et al.* [42] introduced a novel machine learning method for filtering by building a hybrid conditional random field model with both discrete and continuous hidden random variables. The experiments can achieve 3.46% overall error rate, which outperforms the previous best systems. Jahromi *et al.* [43] proposed a novel filtering algorithm using artificial neural network (ANN). They trained the ANN in two different strategies including either semiautomatic selection or manual selection of training data. Experiments demonstrate that both the two strategies could obtain promising results. Recently, a new filtering method based on deep learning using deep convolutional neural networks (CNN) was

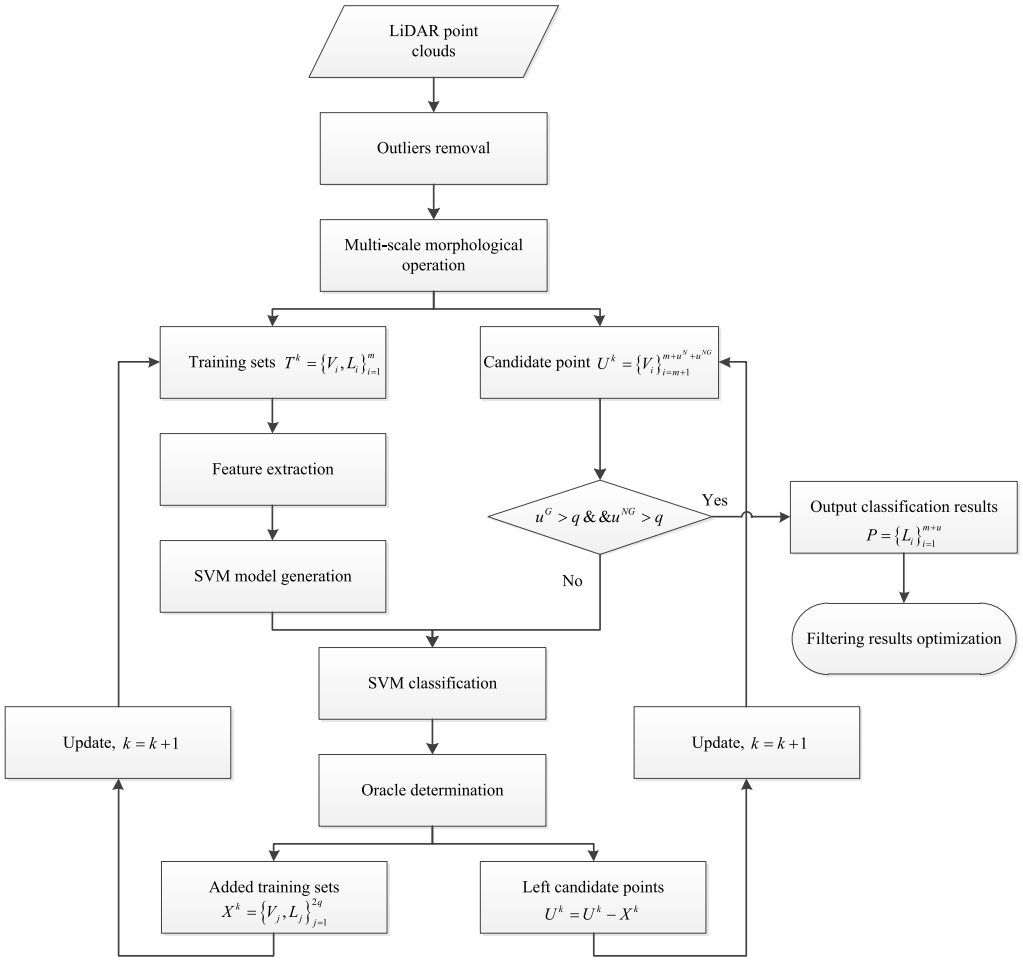

FIGURE 1. The flow chart of the proposed method.

proposed by Hu and Yuan [44] In their method, the classification of a point was considered as the classification of an image. By training with over 17 million labeled points, a deep CNN model with 150 million parameters can be built for filtering. The experimental results showed that the deep CNN model outperforms all the state-of-the-art algorithms in terms of error rate (1.22%). Similarly, Rizaldy *et al.* [45] presented a deep learning approach for ground classification. In their method, the point cloud is initially transformed into a multi-dimensional image. Then, the fully convolutional networks (FCN) with dilated kernels are designed to perform image classification. Experimental results showed that the FCN-based filtering method performed better than the CNN-based filtering method in terms of total error and type I error when only using the ISPRS datasets for training. Although these machine-learning-based approaches seem to be an accurate and easy-to-implement way for filtering, they also have some drawbacks. First of all, these kinds of methods always require lots of labeled points for training, whereas classifying points as ground and non-ground manually may be a huge human work. Moreover, some of these methods cannot achieve good performance in complex terrain environments.

To address the filtering challenges mentioned above, this paper presents an active learning filtering method. In the proposed method, the initial training samples can be selected and labeled automatically using morphological operators. Then, a support vector machine (SVM) model can be built and updated iteratively according to the active learning strategy. The filtering accuracy improved gradually and the filtering results turned better and better. The remainder of this paper is organized as follows. Section 2 elaborates the steps of the proposed method, including removing outliers, obtaining and labeling the initial training samples, point cloud features extraction, oracle design and samples selection, and classification results optimization. In Section 3, the experimental tests are undertaken to evaluate the proposed method and a detailed analysis is made towards the experimental results. Finally, conclusions are drawn at end of this paper.

II. METHODOLOGY

The flow chart of the proposed method is shown in Fig. 1. The outliers are first detected and removed since their abnormal elevation values will affect the subsequent extraction of ground points. To reduce the intervention and release human resources, this paper applies multi-scale

morphological operations to extract and label the training sets automatically. Then, a SVM model is built using several calculated features. According to the SVM model, the candidate points can be classified as ground points and non-ground points. The key for active learning is to define the oracle. In this paper, the oracle is set as a sigmoid function of the residuals from the candidate points to the fitted surface generated using ground points in the training sets. In the iteration, some points from the candidate ground points and non-ground points are selected and labeled as ground points and non-ground points separately according to the oracle. Subsequently, the newly added train samples update the training sets. Meanwhile, these points should be removed from the candidate points. As a consequence, the SVM model can be revised iteratively using the updated training sets. The remaining candidate points are then reclassified using the updated SVM model. The above-mentioned process is iterated until termination test condition is met. Considering the errors caused by the point-based classification, the filtering results are further optimized using a slope based method. The proposed method is mainly composed of the following five steps.

A. REMOVING OUTLIERS

The point clouds generally contain noisy points due to the influence of the instrument itself or the external environment. These noisy points can be categorized into low and high outliers as shown in Fig. 2. The low outliers normally originate from multi-path and errors in the laser range finder and thus do not belong to the landscape. The high outliers are always elevated points that are generally generated by birds and low flying aircraft [4]. The existence of noisy points will always bring about some negative effects, including the following: (1) the quality of DTM generation may be affected by the noisy points, especially the low outliers, since most of the filtering algorithms always assume that the lowest points in the local areas must belong to ground; (2) the rendering of point cloud based on elevation will be influenced due to the maximal or minimal elevations of outliers; and (3) mass of noisy point will incur low three-dimensional model reconstruction quality and decrease the degree of automation. Hence, outliers should first be removed.

To remove outliers, this paper proposes a denoising algorithm based on image processing technique. The flow chart of the proposed method is shown in Tab. 1. Firstly, the three-dimensional point clouds $data\,(x, y, z)$ are transformed into two-dimensional raster grids $DSM\,(i, j)$. The transformation mapping relationship R should be preserved. Subsequently, mean filtering is applied to the $DSM\,(i, j)$ to obtain $\overline{DSM}\,(i, j)$. The filtering results are influenced by the window size. Generally, a large filtering window is easy to flatten terrain details. In such situations, some LiDAR points are prone to be misclassified as outliers. On the contrary, a small filtering window is ineffective to detect outliers. This paper adopts a 5×5 filtering window as the mean filtering by trial and error. Comparing with the difference of the characteristic values of each grid between $DSM\,(i, j)$ and $\overline{DSM}\,(i, j)$, the characteristic value of each grid in $DSM\,(i, j)$ is replaced by that of grid in $\overline{DSM}\,(i, j)$, if the difference is larger than the threshold T_1, as shown in (1):

$$DSM\,(i,j) = \left\{\overline{DSM}\,(i,j)\,\middle|\,abs\left(\overline{DSM}\,(i,j) - DSM\,(i,j)\right) > T_1\right\} \quad (1)$$

where $abs\,(\cdot)$ means the absolute value, T_1 is the threshold. In this paper, T_1 is set to 5, since this constant is able to detect abnormal characteristic values successfully while protecting details from being flattened effectively. Here, the recovered point clouds $data\left(x, y, \hat{z}\right)$ can be obtained by inverse transformation according to the mapping relationship R. Comparing with the difference between the observed elevation z and the recovered elevation $\hat{z}$, the points with larger elevation differences are detected as outliers and removed.

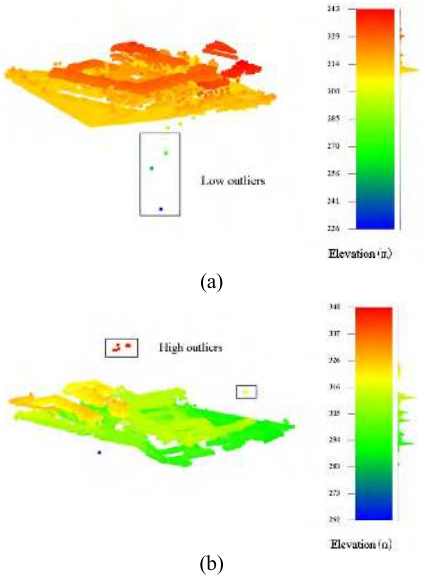

FIGURE 2. Low and high outliers: (a) Low outliers; (b) High outliers.

TABLE 1. Flow chart of the denoising algorithm.

Input: three-dimensional point clouds $data\left(x, y, z\right)$
Steps:
1. Point clouds transformation: $data\left(x, y, z\right) \underset{\Rightarrow}{R} DSM\left(i, j\right)$
2. Mean filtering: $\overline{DSM}\left(i, j\right) = mean\left(DSM\left(i, j\right)\right)$
3. Values updating: $DSM\left(i, j\right) = \left\{\overline{DSM}\left(i, j\right)\middle\vert abs\left(\overline{DSM}\left(i, j\right) - DSM\left(i, j\right)\right) > T_1\right\}$
4. Inverse transformation: $DSM\left(i, j\right) \underset{\Rightarrow}{R} data\left(x, y, \hat{z}\right)$
5. Outlier detection: $noise = \left\{data\left(x_i, y_i, z_i\right)\middle\vert abs\left(z_i - \hat{z}_i\right) > T_2\right\}$
Output: Denoising results $data \leftarrow data \setminus noise$

B. OBTAINING AND LABELING THE INITIAL TRAINING SAMPLES

Although the traditional supervising learning algorithm can obtain good filtering performance, they need huge amounts of labeled training samples. The labeling process is generally time-consuming and needs much human intervention. As a result, the automation of these algorithms is low-level. To solve this problem, this paper adopts multi-scale morphological operations to obtain and label the initial train samples automatically.

The morphological filtering generally involves two basic operations, including morphological dilation and morphological erosion. The morphological dilation D selects the highest elevation value of all the points within the filtering window, while the morphological erosion E selects the lowest elevation value of all the points within the filtering window, given as (2) [46]:

$$\begin{cases} D\left(z_p\right) = \max\limits_{(x_i,y_i)\in W}\left(z_i\right) \\ E\left(z_p\right) = \min\limits_{(x_i,y_i)\in W}\left(z_i\right) \end{cases} \tag{2}$$

where W is the filtering window, (x_i, y_i, z_i) is the point within the filtering window. The morphological opening O is achieved by applying morphological erosion followed by dilation given as (3):

$$O\left(z_p\right) = D\left(E\left(z_p\right)\right) \tag{3}$$

In morphological filtering, the points whose elevation differences are greater than a threshold before and after the morphological opening are detected to be non-ground points. However, adopting different size of filtering window will produce different filtering outcomes. Fig.3 (a) shows two-dimensional terrain features, including terrain, buildings and abrupt terrain. When applying a larger filtering window to filtering, although large buildings can be removed, the terrain details cannot be protected (Fig. 3(b)). Conversely, when using a smaller filtering window, terrain details can be preserved whereas some buildings cannot be filtered out (Fig. 3(c)). From another prospective, when adopting a larger filtering window for filtering, although parts of terrains will be removed, the non-filtered ground points are accurate, as the solid part shown in Fig. 3(b). When using a smaller filtering window, although parts of building cannot be removed, the filtered objects can be seen as accurate non-ground points, as the dashed parts shown in Fig. 3(c). Therefore, when using a large filtering window for filtering, the ground points in the filtering results are selected and labeled as ground training samples. When adopting a smaller filtering window for filtering, the non-ground points in the filtering results are selected and labeled as non-ground training samples. The large filtering window should be greater than the largest object in the test site. Here, a filtering window with 50×50 in size is commonly applicable. However, a larger filtering window such as 60×60 is also appropriate. It should be noted that the size of a large filtering window does not have a significant influence on the final filtering results. To obtain more non-ground training samples, the smallest filtering window with 3×3 in size should be selected.

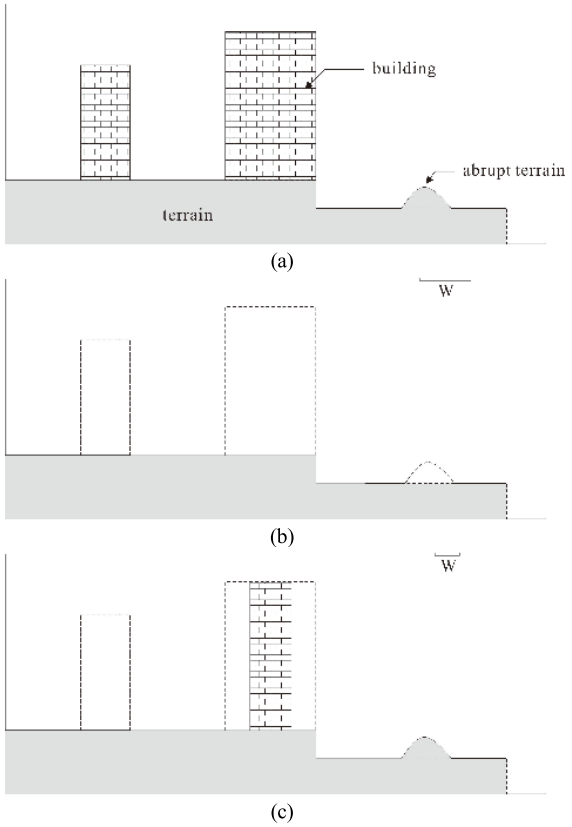

FIGURE 3. Multi-scale morphological filtering results: (a) Two-dimensional terrain features, including terrain, building and abrupt terrain; (b) The filtering results using a larger filtering window; (c) The filtering results using a smaller filtering window. The dash lines indicate the filtered parts.

C. POINT CLOUD FEATURES EXTRACTION

This paper extracts geometric features to build a SVM model, since these features are easily accessible [47]. The geometric features include two parts. One part is calculated based on a local three-dimensional structure covariance tensor, while the other part is achieved based on elevation values of neighboring points.

The raw point clouds are irregularly distributed. To fast locate one point's neighbors, this paper adopts k-dimensional tree to organize the point clouds [48]. To compute the features for a point p, its neighboring point sets $Kn\,(p)$ are first obtained. Then, the local three-dimensional structure covariance tensor Cov_p can be calculated according to (4):

$$Cov_p = \frac{1}{k}\sum_{i=1}^{k}\left(p_i - \bar{p}\right)\left(p_i - \bar{p}\right)^T \tag{4}$$

where p_i is one point in $Kn\,(p)$, k is the number of the neighboring points. k does not have significant influence on the SVM classification results. In this paper, k is set to 10 as

suggested by Becker *et al.* [47]. The $\bar{p}$ is the medoid of $Kn\,(p)$, which can be calculated according to (5):

$$\bar{p} = \arg\min_p \sum_{i=1}^{k} \|p_i - p\| \tag{5}$$

According to Cov_p, three eigenvalues $\lambda_0 \geq \lambda_1 \geq \lambda_2 \geq 0$ can be calculated. Correspondingly, three eigenvectors e_0, e_1 and e_2 can also be obtained. Using these three eigenvalues and three eigenvectors, the features of the first part including anisotropy, planarity, linearity, scatter and surface variation can be calculated as (6)-(10):

$$\text{anisotropy}: \quad (\lambda_0 - \lambda_2)/\lambda_0 \tag{6}$$

$$\text{planarity}: \quad (\lambda_1 - \lambda_2)/\lambda_0 \tag{7}$$

$$\text{linearity}: \quad (\lambda_0 - \lambda_1)/\lambda_0 \tag{8}$$

$$\text{scatter}: \quad \lambda_2/\lambda_0 \tag{9}$$

$$\text{Surfacevariation}: \quad \lambda_2 \tag{10}$$

The other part of geometric features can be calculated according to elevations of neighboring points. These features include vertical range, height below and height above given as (11-13).

$$\text{vertical range}: \quad Z_{\max}\{Kn(p)\} - Z_{\min}\{Kn(p)\} \tag{11}$$

$$\text{height below}: \quad Z_p - Z_{\min}\{Kn(p)\} \tag{12}$$

$$\text{height above}: \quad Z_{\max}\{Kn(p)\} - Z_p \tag{13}$$

where Z_p is the height value of point p. $Z_{\max}(\cdot)$ is the maximum height value of the neighboring point sets $Kn\,(p)$, whereas $Z_{\min}(\cdot)$ is the minimum height value.

D. ORACLE DESIGN AND SAMPLES SELECTION

In active learning, the learner should actively query an oracle outside the learner to get the labels for the samples. Thus, to obtain a good classification result, it is necessary to set the oracle correctly and appropriately.

In this paper, the oracle is set to a sigmoid function of the residual between the point and the fitted surface given as (14)

$$\begin{cases} f\,(p) = Z_p - \sum_{i=1}^{n} \lambda_i \phi\,(\|p - p_i\|) \\ S\,(f) = \dfrac{1}{1 + e^{-f}} \end{cases} \tag{14}$$

where p is the candidate point, z_p is the observed elevation value, $\sum_{i=1}^{n} \lambda_i \phi\,(\|p - p_i\|)$ is to generate a fitted surface according to the radial basis function (RBF). $f\,(p)$ is the residue between the point p and the fitted surface as shown in Fig. 4.

The flow chart of the active learning is shown in Tab. 2. In each iteration, q points with smallest $S\,(f)$ values are selected from the candidate ground point sets $\{G\}^k$ and are added into ground training samples. Meanwhile, q points with largest $S\,(f)$ values are selected from the candidate non-ground point sets $\{NG\}^k$ and are added into non-ground training samples. The training model is updated using these new training samples. This process is iterated until the number of points in $\{G\}^k$ and $\{NG\}^k$ is no longer larger than q. q does not have a strong influence on the performance of the presented approach. q mainly affects the iteration times. Considering efficiency, q was set to 1000 in this paper.

Note that the training samples mentioned in Tab. 2 include two parts, one is the initial training samples obtained at subsection B, the other is the added training samples generated iteratively based on the principles referred to subsection D. The training sets and the testing sets are two different components. The training sets do not overlap the testing sets.

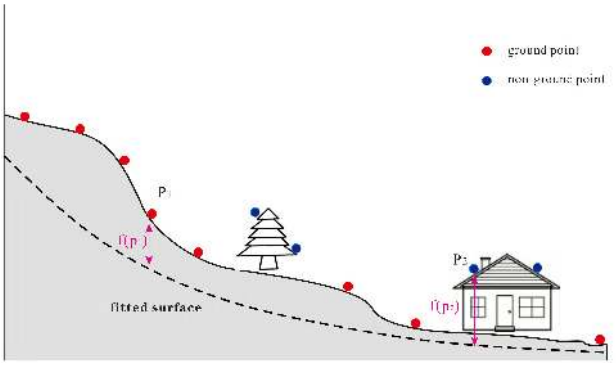

FIGURE 4. The schematic diagram of oracle setting. The dash line represents a fitted surface. The red points are ground points while the blue points are object points.

TABLE 2. Flow chart of the active learning.

Point cloud filtering based on active learning:

Input:

1. Initial training samples $T^k = \{V_i, L_i\}_{i=1}^{m}$, V_i is the point p_i's geometric features, L_i is the corresponding label for each training point, in which 0 represents a ground point while 1 represents a non-ground point. m is the number of training samples, k is the number of iterations which is initialized to be 1.

2. Candidate classification point sets $U^k = \{V_i\}_{i=m+1}^{m+u}$, u is the total number of the candidate points.

Repeat:

1. Adopting the training samples $T^k = \{V_i, L_i\}_{i=1}^{m}$ to build a Support Vector Machine (SVM) training model and use it to classify U^k as $\{G\}^k$ and $\{NG\}^k$. The number of these two sets is u^G and u^{NG}, respectively.

2. According to the oracle setting method, calculate $S(f)$ of each point in $\{G\}^k$ and $\{NG\}^k$, respectively.

3. Select q points with smallest $S(f)$ values from T^k. Meanwhile, $k = k + 1$.

4. If u^G and u^{NG} are both greater than q, keep iterating steps 1-3; otherwise, break.

End

Output:

Point clouds classification results $P = \{L_i\}_{i=1}^{m+u}$

E. CLASSIFICATION RESULTS OPTIMIZATION

Considering the errors caused by the point-based classification, this paper uses a slope-based method to optimize the classification results. As shown in Fig. 5 (a), it is a digital terrain model (DTM) generated using the ground points classified by the SVM model. To fine-tune the filtering results, this paper first divides the filtering results into grids as shown in Fig. 5 (b). Subsequently, the lowest point in each grid is selected to be a ground seed. All the ground seeds are used to interpolate a fitted surface according to the RBF interpolator as shown in Fig. 5 (c). Moreover, the fitted elevation $\hat{z}_i$ for each point can be calculated. According to the fitted surface, the slope gradient in x and y directions $\left(s_i^u, s_i^v\right)$ can also be obtained. The points that satisfy (15) are determined as non-ground points and removed.

$$non\_gps = \left\{ p_i \left| z_i - \hat{z}_i > te + \left(\left(s_i^u\right)^2 + \left(s_i^v\right)^2 \right), i = 1, 2, \cdots, n \right. \right\} \tag{15}$$

where z_i is the observed elevation, $\hat{z}_i$ is the corresponding fitted elevation, te is a constant that is set to 0.3 in this paper, since 0.3 m is appropriate to discriminate low vegetation from grounds.

III. EXPERIMENTAL RESULTS AND ANALYSIS

This paper adopts three publicly available datasets provided by the ISPRS to test the performance of the proposed method [28]. These three datasets are acquired using an Optech ALTM laser scanner and the point space is 1 m- 1.5 m. These three datasets are selected since they include different terrain features and filtering challenges. Thus, it is helpful to test the filtering performance in different terrain environments. As shown in Fig. 6 (a), the terrain slope varies greatly in the first dataset (sample 1) and there is some low vegetation on the slope. Moreover, some parts of the buildings are attached to the terrains. These points are easy to be misclassified as ground points. In the second dataset (sample 2), the main filtering challenges are complex buildings as shown in Fig. 6 (b). How to remove larger objects (such as the buildings) and smaller objects (such as cars and pedestrians) simultaneously is a filtering difficulty. In the third dataset (sample 3), it is difficult for most filtering algorithms to discriminate the attached objects (such as the bridge in the Fig. 6 (c)) from the terrains, since their elevations are close to each other. Thus, these datasets are representative to test the filtering performance in different terrain environments.

In Figs. 7-9, (a) is the digital surface model (DSM) generated using point clouds in each sample; (b) is the true digital terrain model (DTM) generated using accurate ground points selected manually; (c) is the extracted DTM generated using the filtered ground points. It can be seen from the comparison that the filtering results are close to the reference ground points. The proposed method can achieve good filtering performances in all the three samples. As shown in Fig. 7(a), there is much low vegetation on the slope. After filtering, both

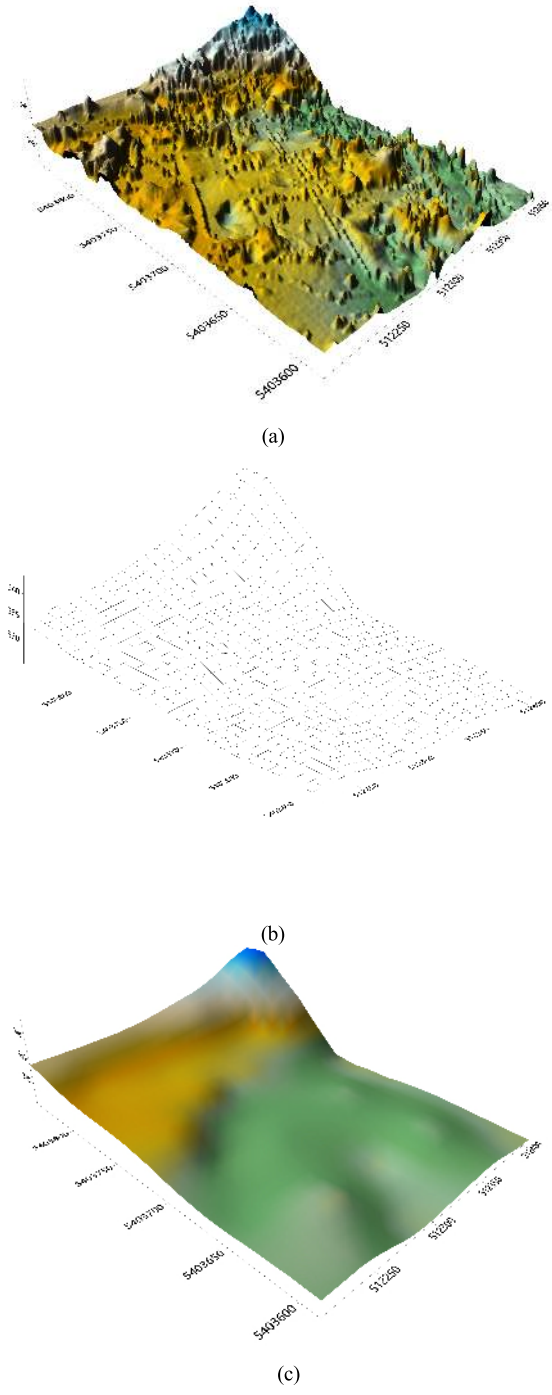

FIGURE 5. Schematic diagram of optimization principle: (a) Digital terrain model generated from ground points classified by SVM model; (b) Divides the filtering results into grids; (c) Interpolate a fitted surface according to the RBF interpolator.

these vegetation and building roofs are correctly classified (Figs 7. (b) and (c)). In sample 2, some small objects are mixed with large buildings as shown in Fig. 8 (a). Comparing with the true ground points (Fig. 8 (b)), the filtering results still contains some commission errors as shown in Fig. 8 (c). These commission errors are mainly caused by cars or pedestrians on the street since their elevations are close to the ones of terrain. In sample 3, the filtering challenge is the attached

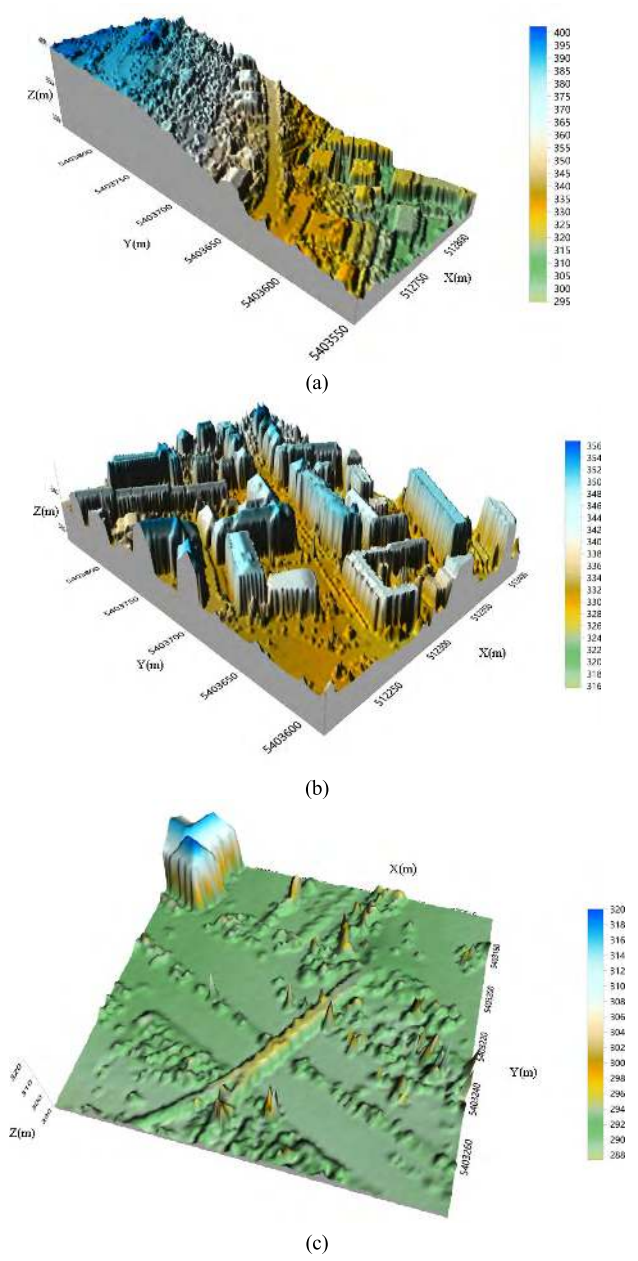

FIGURE 6. Terrain features of the three datasets: (a) Terrain features of sample 1; (b) Terrain features of sample 2; (c) Terrain features of sample 3.

object (bridge) as shown in Fig. 9 (a). The filtered DTM is very close to the reference DTM (Fig. 9 (b) and Fig. 9 (c)). It can be concluded that the proposed method achieves the best filtering performance towards sample 3.

This paper adopts three accuracy indexes including type I error, type II error and total error to access the filtering effect of the proposed method. Type I error also referred to as omission error is the percentage of ground points misclassified as non-ground points. Type II error also called as commission error is the percentage of non-ground points accepted as ground points. Total error is percentage of all the misclassified points. A confusion matrix towards these three kinds of errors is tabulated in Tab. 3. Type I, type II and total

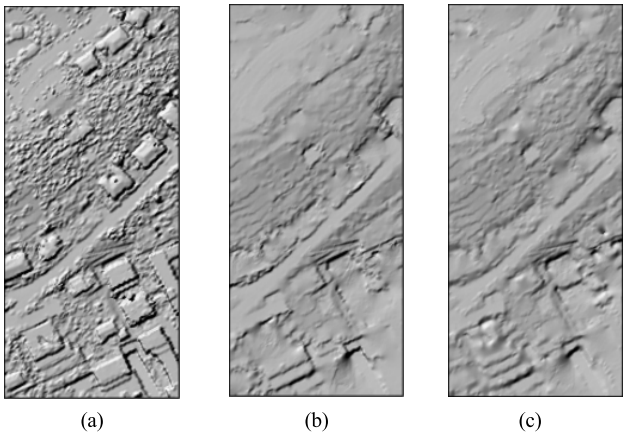

FIGURE 7. Filtering performance of sample 1: (a) DSM before filtering; (b) True DTM generated using reference ground points; (c) Extracted DTM generated using the filtering results.

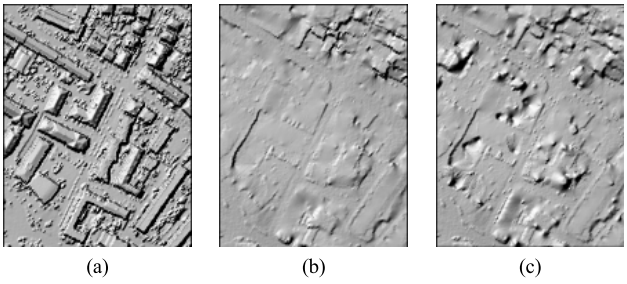

FIGURE 8. Filtering performance of sample 2: (a) DSM before filtering; (b) True DTM generated using reference ground points; (c) Extracted DTM generated using the filtering results.

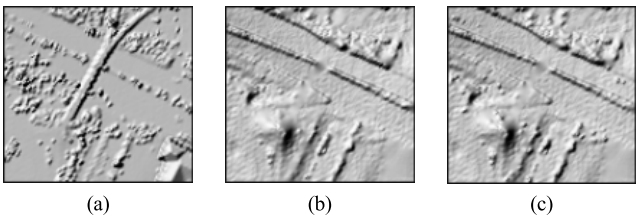

FIGURE 9. Filtering performance of sample 3: (a) DSM before filtering; (b) True DTM generated using reference ground points; (c) Extracted DTM generated using the filtering results.

errors were calculated using (16)-(18).

$$T_1 = b/(a+b) \tag{16}$$

$$T_2 = c/(c+d) \tag{17}$$

$$total = (a+b)/(a+b+c+d) \tag{18}$$

Three types of errors in the tested datasets of the proposed method and the ones of some famous filtering algorithms proposed in recent years are shown in Tabs. 4-6. Jahromi *et al.* [43] applied artificial neural network (ANN) to filtering and obtained good filtering performances. Mongus and alik [24] used thin plate spline (TPS) interpolator for filtering. Zhang and Lin [29] modified the traditional PTD filtering method by segmenting the point clouds firstly. Li *et al.* [20] proposed an improved top-hat filtering method to protect terrain details. Hui *et al.* [21] combined the

TABLE 3. Confusion matrix of the three types of errors.

		Filtering results	
		Ground	Non-ground
Reference results	Ground	*a*	*b*
	Non-ground	*c*	*d*

TABLE 4. comparison of total errors (%).

	Sample 1	Sample 2	Sample 3	Ave
Jahromi (2011)	19.83	6.10	2.75	9.56
Mongus (2012)	11.01	5.17	1.98	6.05
Zhang (2013)	18.49	5.92	4.95	9.79
Li (2014)	14.18	3.26	2.55	6.66
Hui (2016)	13.34	3.5	2.21	6.35
Zhang (2016)	12.01	2.97	3.42	6.13
Hu (2016)	19.47	7.99	2.23	9.90
Li (2017)	12.67	3.54	1.82	6.01
Ni (2018)	18.19	8.83	7.9	11.64
Rizaldy (2018)	15.01	3.44	1.6	6.68
Proposed method	11.03	4.28	1.23	5.51

TABLE 5. Comparison OF type I errors (%).

	Sample 1	Sample 2	Sample 3	Ave
Jahromi (2011)	29.10	9.97	2.92	14.00
Mongus (2012)	7.32	4.23	0.01	3.85
Zhang (2013)	25.67	8.13	1.17	11.66
Li (2014)	20.43	3.66	2.39	8.83
Hui (2016)	13.63	4.86	0.01	6.17
Zhang (2016)	7.23	1.15	3.89	4.09
Hu (2016)	27.1	13.92	1.63	14.22
Li (2017)	12.04	1.95	0.73	4.91
Ni (2018)	18.01	5.95	8.81	10.92
Rizaldy (2019)	14.09	2.52	0.24	5.62
Proposed method	14.14	3.41	2.48	6.68

traditional surface-based filtering method and the traditional morphological filtering method to obtain better filtering results. Zhang *et al.* [22] proposed an easy-to-use filtering method based on cloth simulation. Hu and Yuan [44] applied CNN to filtering and achieved good filtering performances. Note that the three errors tabulated in Tabs. 4-6 are the CNN classifier using ten samples for training. When adopting 17 million points for training, the CNN classifier can achieve much smaller filtering errors (2.26% of type I error, 1.22% of type II error and 0.67% of total error). Li *et al.* [1] presented a filtering method based on geodesic transformations of mathematical morphology. Ni *et al.* [49] adopted graph cuts for filtering. Rizaldy *et al.* [45] applied FCN to filtering, in which good filtering results can be achieved with few training samples.

TABLE 6. Comparison of type II errors (%).

	Sample 1	Sample 2	Sample 3	Ave
Jahromi (2011)	7.44	1.99	2.19	3.87
Mongus (2012)	15.98	6.15	8.87	10.33
Zhang (2013)	8.84	3.61	18.23	10.23
Li (2014)	5.78	2.84	3.13	3.92
Hui (2016)	12.96	2.08	9.95	8.33
Zhang (2016)	18.44	4.9	1.78	8.37
Hu (2016)	9.2	1.75	4.39	5.11
Li (2017)	13.52	5.21	5.63	8.12
Ni (2018)	18.44	11.85	4.73	11.67
Rizaldy (2019)	16.25	4.41	6.53	9.06
Proposed method	8.56	5.08	0.88	4.84

From Tab.4, it can be found that the proposed method can obtain the smallest average total error (5.51%) compared to other ten methods. In the ten methods, the largest average total error is 11.64% which is twice of that of this method. Thus, the proposed method can achieve the best filtering performance. Furthermore, the total errors in three samples of the proposed method are all smaller except sample 2. It can be concluded that this method owns strong adaptability to different terrain environments. From Tabs. 5 and 6, it can be seen that the average type I error (6.68%) and the average type II error (4.84%) are close with each other. This indicates that the proposed method in this paper can not only effectively remove the ground points but also effectively protect the terrain details from being destroyed. On the contrary, the average type I error of the method proposed by Jahromi *et al.* [43] is 14.00% while its average type II error is 3.87%. Moreover, the average type I error of the method proposed by Mongus and alik [24] is 3.85% while its average type II error is 10.33 %. These two methods were selected because Jahromi *et al.* [43] achieved the smallest average type II error, while Mongus and alik [24] performed the best in terms of the average type I error. It can be found that these methods cannot balance these two errors. In other words, these methods have no capability to preserve the details of terrains as much as possible while reducing the interferences from the non-ground points.

Fig. 10 is the type I and type II errors distributions of the three tested samples. From Fig. 10 (a), it can be found that both the type I and type II errors in sample 1 are a little larger. This is because the terrain slope of sample 1 changes greatly and some parts of the abrupt terrains are rejected as non-ground points which form the type I error. Moreover, some roofs of buildings are connected to the terrains making these points to be easily misclassified as ground points thereby yielding to larger type II errors. Fig. 10 (b) shows that the main filtering error in sample 2 is type II error which is caused by some small objects. In sample 3, the filtering result is very close to the reference result with only a few points misclassified (Fig. 10 (c)). Thus, the total error of sample 3 is very

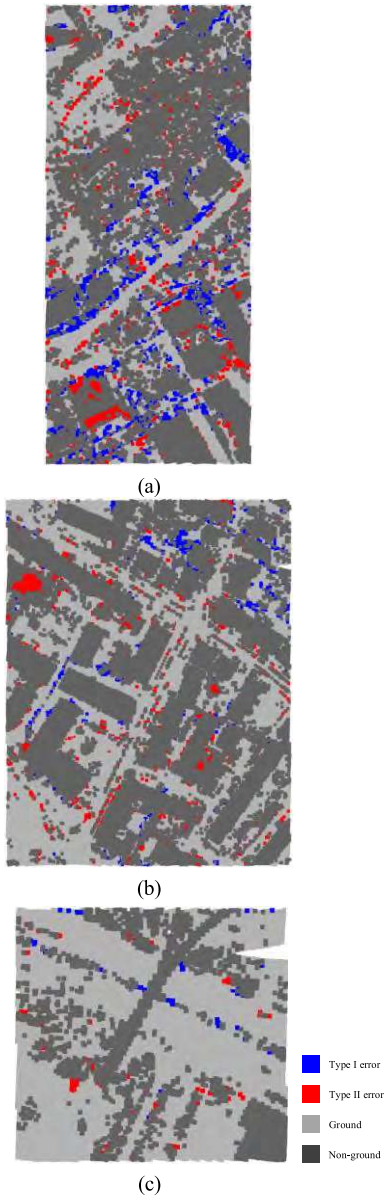

FIGURE 10. Error distributions of the three samples: (a) Error distributions of sample 1; (b) Error distributions of sample 2; (c) Error distributions of sample 3. The blue grids represent type I error, while the red grids are type II error. The light gray grids indicate the points rightly classified as ground points, while the dark gray grids are the points rightly classified as non-ground points.

small (1.23% in Tab. 4). From these three filtering results, it can be seen that the proposed method performs better in flat terrains. This characteristic is also consistent with most other filtering methods.

IV. DISCUSSION

The proposed method involves five main steps, including removing outliers, obtaining and labeling the initial training samples, point cloud features extraction, oracle design and samples selection, and classification results optimization. Among these five steps, obtaining and labeling the initial training samples and point cloud features extraction are mandatory steps, whereas the other three steps can be seen as optimization steps. Thus, for analyzing contributions of different pipeline components, this paper conducted the following ablation study:

i What will be the filtering results without outliers removal?

ii What will be the filtering results without oracle design and samples selection?

iii What will be the filtering results without classification results optimization?

The filtering results of the above-mentioned three ablation studies are shown in Tabs. 7-9. Comparing with the three types of errors listed in Tabs. 4-6, it can be found that all the errors of the three samples turn larger without the optimization steps. These include removing outliers, oracle design and samples selection, and classification results optimization. From Tab. 7, it can be seen that the total errors of the three samples are slightly larger without outlier removal. It can be concluded that the outliers indeed have influence on the filtering results. Therefore, removing outliers first can improve the filtering performance. The filtering results in Tab. 8 are obtained using the initial training samples. It can be found that the proposed method does not perform well in these samples, especially for sample 1, whose total error is almost twice of that of using oracle design and samples selection. In this paper, the step of oracle design and samples selection is to acquire more labeled samples iteratively. In so doing, the SVM model can be revised from coarse to better. Therefore, this step is crucial for the proposed method. From Tab. 9, it is easy to see that the proposed method is prone to achieve unbalanced type I and type II errors without the step of classification results optimization. For instance, the type I error of sample 2 is 0.1%, while its type II error is 30.65%. The type II error of sample 3 is 0.03%, whereas its type I error

TABLE 7. Filtering results of ablation study i.

Samples	Total (%)	T1 (%)	T2 (%)
Sample 1	11.06	13.07	9.56
Sample 2	4.84	2.76	6.65
Sample 3	2.09	5.35	1.15

TABLE 8. Filtering results of ablation study ii.

Samples	Total (%)	T1 (%)	T2 (%)
Sample 1	20.84	18.44	22.11
Sample 2	5.88	2.76	7.75
Sample 3	3.09	1.14	3.56

TABLE 9. Filtering results of ablation study iii.

Samples	Total (%)	T1 (%)	T2 (%)
Sample 1	11.37	10.23	12.91
Sample 2	15.33	0.1	30.65
Sample 3	12.57	16.14	0.03

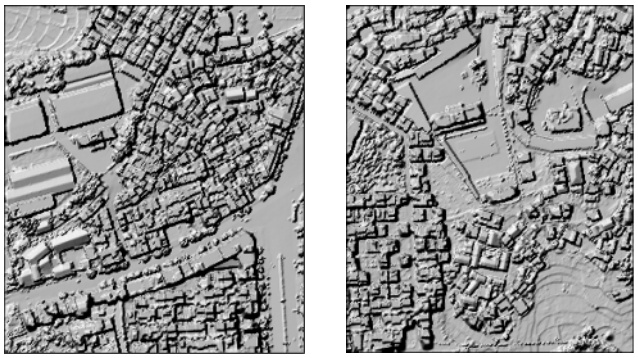

FIGURE 11. Topography and landforms of the two datasets used in practice: (a) dataset 1 from Luoding, China; (b) dataset 2 from Luoding, China.

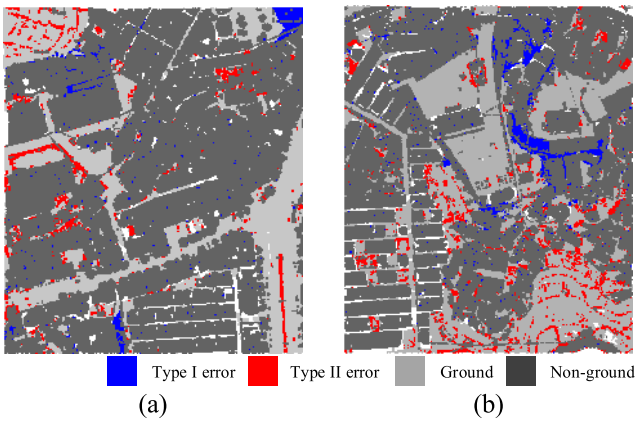

FIGURE 12. Error distributions of the two datasets used in practice: (a) Error distributions of dataset 1; (b) Error distributions of dataset 2. Note that in these two figures there are some white components that are generated since these parts are data gaps.

is 16.14%. As a result, all the total errors of the three samples are larger. This is because the SVM classification used in this paper is based on the point primitive. It is very error-prone when calculating geometric features for each point. Hence, the step of classification results optimization is very important to achieve good filtering performances.

To better show the generalization of the presented approach, two different datasets used in practice other than the widely used ISPRS data [28] were tested. The new datasets are located within the city of Luoding, China, characterized by modern architecture with low and high-storey buildings as shown in Fig. 11 (a) and (b). The datasets were obtained by an ALS50 scanner with an average point density of 2.76 points/m^2. In terms of the first datasets (Fig. 11a), the type I, type II and total errors are 8.34%, 2.99%, and 4.81%, respectively. In terms of the second datasets (Fig. 11b), the type I, type II and total errors are 8.76%, 6.19%, and 7.39%, respectively. Graphical illustrations of the type I and type II error distributions of the two datasets are shown in Fig. 12 (a) and (b). From the error calculation results and distributions, it can be found that the proposed method performed well on the airborne LiDAR datasets (Fig. 11 a and b) even though the datasets contained a large number of points with high point density.

V. CONCLUSION

Airborne LiDAR filtering is a critical step in point cloud post-processing applications. To solve the problems of low filtering accuracy in complex terrain environments and excessive human intervention, this paper proposed a filtering algorithm based on active learning. In this method, multi-scale morphological filtering methods are adopted to obtain and label the initial training samples. This paper then applies the active learning strategy to add training samples gradually and update the SVM model progressively. Finally, this paper adopts the slope-based method to optimize the classification results. The proposed method has been tested using the three datasets provided by the ISPRS. The experimental results showed that the total errors of the proposed method were smaller. This indicates that the method can achieve good filtering performances in different terrain environments. Moreover, the average total error of the proposed method is the smallest when comparing with that of other ten famous filtering methods. In terms of average type I and type II errors, the proposed method can balance these two types of errors. Thus, the proposed method can filter out non-ground points as more as possible while preserving terrain details. Overall, this paper realizes the automatic classification of point clouds without manually selecting training samples and labeling. This feature greatly reduces the human intervention and improves the degree of algorithm automation. Furthermore, the proposed method can adapt to different terrain environments and achieve good filtering performances.

REFERENCES

[1] Y. Li, B. Yong, P. Van Oosterom, M. Lemmens, H. Wu, L. Ren, M. Zheng, and J. Zhou, "Airborne LiDAR data filtering based on geodesic transformations of mathematical morphology," *Remote Sens.*, vol. 9, no. 11, p. 1104, Oct. 2017.

[2] Z. Hui, L. Wang, Y. Y. Ziggah, S. Cai, and Y. Xia, "Automatic morphological filtering algorithm for airborne LiDAR data in urban areas," *Appl. Opt.*, vol. 58, no. 4, pp. 1164–1173, 2019.

[3] Z. Chen, B. Gao, and B. Devereux, "State-of-the-art: DTM generation using airborne LiDAR data," *Sensors*, vol. 17, no. 1, p. 150, Jan. 2017.

[4] Z. Hui, D. Lia, S. Jin, Y. Y. Ziggah, L. Wang, and Y. Hu, "Automatic DTM extraction from airborne LiDAR based on expectation-maximization," *Opt. Laser Technol.*, vol. 112, pp. 43–55, Apr. 2019.

[5] Z. Hui, Y. Hu, S. Jin, and Z. Y. Yevenyo, "Road centerline extraction from airborne LiDAR point cloud based on hierarchical fusion and optimization," *ISPRS J. Photogram. Remote Sens.*, vol. 118, pp. 22–36, Aug. 2016.

[6] A. Matkan, M. Hajeb, and S. Sadeghian, "Road extraction from lidar data using support vector machine classification," *Photogramm. Eng. Remote Sens.*, vol. 80, pp. 409–422, May 2014.

[7] J. Zhang, X. Lin, and X. Ning, "SVM-based classification of segmented airborne LiDAR point clouds in urban areas," *Remote Sens.*, vol. 5, no. 8, pp. 3749–3775, Jul. 2013.

[8] S. Xu, G. Vosselman, and S. O. Elberink, "Multiple-entity based classification of airborne laser scanning data in urban areas," *ISPRS J. Photogram. Remote Sens.*, vol. 88, pp. 1–15, Feb. 2014.

[9] C. Véga, J. P. Renaud, S. Durrieu, and M. Bouvier, "On the interest of penetration depth, canopy area and volume metrics to improve Lidar-based models of forest parameters," *Remote Sens. Environ.*, vol. 175, pp. 32–42, Mar. 2016.

[10] L. Xinlian *et al.*, "International benchmarking of terrestrial laser scanning approaches for forest inventories," *ISPRS J. Photogram. Remote Sens.*, vol. 144, pp. 137–179, Oct. 2018.
[11] P. Cheng, Z. Hui, Y. Xia, Y. Ziggah, Y. Hu, and J. Wu, "An improved skewness balancing filtering algorithm based on thin plate spline interpolation," *Appl. Sci.*, vol. 9, no. 1, p. 203, Jan. 2019.
[12] X. Meng, N. Currit, and K. Zhao, "Ground filtering algorithms for airborne LiDAR data: A review of critical issues," *Remote Sens.*, vol. 2, no. 3, pp. 833–860, Mar. 2010.
[13] G. Vosselman, "Slope based filtering of laser altimetry data," *Int. Arch. Photogram., Remote Sens. Spatial Inf. Sci.*, vol. 33, pp. 935–942, Jul. 2000.
[14] G. Sithole, "Filtering of laser altimetry data using slope adaptive filter," *Int. Arch. Photogram., Remote Sens. Spatial Inf. Sci.*, vol. 34, pp. 203–210, Oct. 2001.
[15] J. Susaki, "Adaptive slope filtering of airborne LiDAR data in urban areas for digital terrain model (DTM) generation," *Remote Sens.*, vol. 4, no. 6, pp. 1804–1819, 2012.
[16] Y. He, C. Zhang, and C. S. Fraser, "Progressive filtering of airborne LiDAR point clouds using graph cuts," *IEEE J. Sel. Topics Appl. Earth Observ. Remote Sens.*, vol. 11, no. 8, pp. 2933–2944, Aug. 2018.
[17] K. Q. Zhang, S. C. Chen, D. Whitman, M. L. Shyu, J. H. Yan, and C. C. Zhang, "A progressive morphological filter for removing nonground measurements from airborne LiDAR data," *IEEE Trans. Geosci. Remote Sens.*, vol. 41, no. 4, pp. 872–882, Apr. 2003.
[18] Q. Chen, P. Gong, D. Baldocchi, and G. Xie, "Filtering airborne laser scanning data with morphological methods," *Photogramm. Eng. Remote Sens.*, vol. 73, pp. 175–185, Feb. 2007.
[19] T. J. Pingel, K. C. Clarke, and W. A. McBride, "An improved simple morphological filter for the terrain classification of airborne LiDAR data," *ISPRS J. Photogram. Remote Sens.*, vol. 77, pp. 21–30, Mar. 2013.
[20] Y. Li, B. Yong, H. Wu, R. An, H. Xu, J. Xu, and Q. He, "Filtering airborne lidar data by modified white top-hat transform with directional edge constraints," *Photogramm. Eng. Remote Sens.*, vol. 80, pp. 133–141, Feb. 2014.
[21] Z. Hui, Y. Hu, Y. Z. Yevenyo, and X. Yu, "An improved morphological algorithm for filtering airborne LiDAR point cloud based on multi-level kriging interpolation," *Remote Sens.*, vol. 8, no. 1, p. 35, Jan. 2016.
[22] W. Zhang, J. Qi, P. Wan, H. Wang, D. Xie, X. Wang, and G. Yan, "An easy-to-use airborne LiDAR data filtering method based on cloth simulation," *Remote Sens.*, vol. 8, no. 6, p. 501, Jun. 2016.
[23] K. Kraus and N. Pfeifer, "Determination of terrain models in wooded areas with airborne laser scanner data," *ISPRS J. Photogram. Remote Sens.*, vol. 53, no. 4, pp. 193–203, Aug. 1998.
[24] D. Mongus and B. alik, "Parameter-free ground filtering of LiDAR data for automatic DTM generation," *ISPRS J. Photogram. Remote Sens.*, vol. 67, pp. 1–12, Jan. 2012.
[25] C. Chen, Y. Li, W. Li, and H. Dai, "A multiresolution hierarchical classification algorithm for filtering airborne LiDAR data," *ISPRS J. Photogram. Remote Sens.*, vol. 82, pp. 1–9, Aug. 2013.
[26] H. Hu, Y. Ding, Q. Zhu, B. Wo, H. Liu, Z. Du, and Y. Zhang, "An adaptive surface filter for airborne laser scanning point clouds by means of regularization and bending energy," *ISPRS J. Photogram. Remote Sens.*, vol. 92, pp. 98–111, Jun. 2014.
[27] P. Axelsson, "DEM generation from laser scanner data using adaptive TIN models," *Int. Arch. Photogramm. Remote Sens.*, vol. 33, no. 4, pp. 110–117, 2000.
[28] G. Sithole and G. Vosselman, "Experimental comparison of filter algorithms for bare-Earth extraction from airborne laser scanning point clouds," *ISPRS J. Photogram. Remote Sens.*, vol. 59, nos. 1–2, pp. 85–101, Aug. 2004.
[29] J. Zhang and X. Lin, "Filtering airborne LiDAR data by embedding smoothness-constrained segmentation in progressive TIN densification," *ISPRS J. Photogram. Remote Sens.*, vol. 81, pp. 44–59, Jul. 2013.
[30] X. Zhao, Q. Guo, Y. Su, and B. Xue, "Improved progressive TIN densification filtering algorithm for airborne LiDAR data in forested areas," *ISPRS J. Photogram. Remote Sens.*, vol. 117, pp. 79–91, Jul. 2016.
[31] D. Tóvári and N. Pfeifer, "Segmentation based robust interpolation—A new approach to laser data filtering," in *Proc. Int. Arch. Photogram., Remote Sens. Spatial Inf. Sci.*, Sep. 2005, pp. 79–84.
[32] X. Lin and J. Zhang, "Segmentation-based filtering of airborne LiDAR point clouds by progressive densification of terrain segments," *Remote Sens.*, vol. 6, no. 2, pp. 1294–1326, Feb. 2014.
[33] C. Chen, Y. Li, C. Yan, H. Dai, G. Liu, and J. Guo, "An improved multi-resolution hierarchical classification method based on robust segmentation for filtering ALS point clouds," *Int. J. Remote Sens.*, vol. 37, no. 4, pp. 950–968, 2016.
[34] A. H. Özcan and C. Ünsalan, "LiDAR data filtering and DTM generation using empirical mode decomposition," *IEEE J. Sel. Topics Appl. Earth Observ. Remote Sens.*, vol. 10, no. 1, pp. 360–371, Jan. 2017.
[35] M. Bartels, H. Wei, and D. C. Mason, "DTM generation from LiDAR data using skewness balancing," in *Proc. 18th Int. Conf. Pattern Recognit. (ICPR)*, Aug. 2006, pp. 566–569.
[36] Y. Bao, C. Cao, C. Chang, X. Li, E. Chen, and Z. Li, "Segmentation to the point clouds of LIDAR data based on change of Kurtosis," *Proc. SPIE*, vol. 6623, Mar. 2008, Art. no. 66231N.
[37] B. Yunfei, L. Guoping, C. Chunxiang, L. Xiaowen, Z. Hao, H. Qisheng, B. Linyan, and C. Chaoyi, "Classification of lidar point cloud and generation of DTM from LiDAR height and intensity data in forested area," in *Proc. Int. Archives Photogram., Remote Sens. Spatial Inf. Sci.*, 2008, pp. 313–318.
[38] M. Bartels and H. Wei, "Threshold-free object and ground point separation in LiDAR data," *Pattern Recognit. Lett.*, vol. 31, no. 10, pp. 1089–1099, Jul. 2010.
[39] M. Elmqvist, "Surface estimation from airborne laser scanner data using active shape models," in *Proc. Int. Arch. Photogram. Remote Sens. Spatial Inf. Sci.*, Sep. 2002, pp. 114–118.
[40] X. Hu, L. Ye, S. Pang, and J. Shan, "Semi-global filtering of airborne LiDAR data for fast extraction of digital terrain models," *Remote Sens.*, vol. 7, no. 8, pp. 10996–11015, Aug. 2015.
[41] S. Ural and J. Shan, "A min-cut based filter for airborne LiDAR data," in *Proc. Int. Arch. Photogramm., Remote Sens. Spatial Inf. Sci. (ISPRS)*, Jul. 2016, pp. 395–401.
[42] W. Lu, K. P. Murphy, J. J. Little, A. Sheffer, and H. Fu, "A hybrid conditional random field for estimating the underlying ground surface from airborne LiDAR data," *IEEE Trans. Geosci. Remote Sens.*, vol. 47, no. 8, pp. 2913–2922, Aug. 2009.
[43] A. B. Jahromi, M. J. V. Zoej, A. Mohammadzadeh, and S. Sadeghian, "A novel filtering algorithm for bare-earth extraction from airborne laser scanning data using an artificial neural network," *IEEE J. Sel. Topics Appl. Earth Observ. Remote Sens.*, vol. 4, no. 4, pp. 836–843, Dec. 2011.
[44] X. Hu and Y. Yuan, "Deep-learning-based classification for DTM extraction from ALS point cloud," *Remote Sens.*, vol. 8, no. 9, p. 730, Sep. 2016.
[45] A. Rizaldy, C. Persello, C. Gevaert, S. Elberink, and G. Vosselman, "Ground and multi-class classification of airborne laser scanner point clouds using fully convolutional networks," *Remote Sens.*, vol. 10, no. 11, p. 1723, Oct. 2018.
[46] Z. Hui, B. Wu, Y. Hu, and Y. Y. Ziggah, "Improved progressive morphological filter for digital terrain model generation from airborne LiDAR data," *Appl. Opt.*, vol. 56, no. 34, pp. 9359–9367, 2017.
[47] C. Becker, E. Rosinskaya, N. Häni, E. D'Angelo, and C. Strecha, "Classification of aerial photogrammetric 3D point clouds," *Photogramm. Eng. Remote Sens.*, vol. 84, no. 5, pp. 287–295, May 2018.
[48] J. L. Bentley, J. H. Friedman, and R. A. Finkel, "An algorithm for finding best matches in logarithmic time," *ACM Trans. Math. Softw.*, vol. 3, pp. 209–226, Sep. 1977.
[49] H. Ni, X. Lin, J. Zhang, D. Chen, and J. Peethambaran, "Joint clusters and iterative graph cuts for ALS point cloud filtering," *IEEE J. Sel. Topics Appl. Earth Observ. Remote Sens.*, vol. 11, no. 3, pp. 990–1004, Mar. 2018.

ZHENYANG HUI was born in Kaifeng, Henan, China, in 1989. He received the B.S. degree in surveying engineering from the Henan University of Engineering, Zhengzhou, Henan, in 2008, and the Ph.D. degree in geodesy and survey engineering from the China University of Geosciences, Wuhan, Hubei, China, in 2017. He has been a Lecturer with the Faculty of Geomatics, East China University of Technology, and a Postdoctoral Researcher with the School of Remote Sensing and Geomatics Engineering, Nanjing University of Information Science and Technology, since 2018. He has published around 20 papers in various journals and conferences. His research interests include LiDAR point clouds processing, artificial intelligence, machine learning, and pattern recognition.

SHUANGGEN JIN (M'05) was born in Anhui, China, in 1974. He received the B.Sc. degree in geodesy from Wuhan University, Wuhan, China, in 1999, and the Ph.D. degree in geodesy from the University of Chinese Academy of Sciences, Beijing, China, in 2003.

He is currently a Professor and the Dean of the School of Remote Sensing and Geomatics Engineering, Nanjing University of Information Science and Technology, China, and a Professor with the Shanghai Astronomical Observatory, CAS, Shanghai, China. His main research interests include satellite navigation, remote sensing, space geodesy, and space/planetary exploration. He has over 400 papers in peer-reviewed journals and proceedings, eight patents/software copyrights, and eight books/monographs with more than 4500 citations and over 40 H-index.

Dr. Jin was a Fellow of IAG, in 2011. He was a member of the Russian Academy of Natural Sciences, in 2017, and the European Academy of Sciences, in 2018, and an IUGG Fellow, in 2019. He has been Editorial Board Member of *GPS Solutions*, since 2016, *Journal of Geodynamics*, since 2014, and *Planetary and Space Science*, since 2014. He has received one First-Class and four Second-Class Prizes of Provincial Awards and the 100-Talent Program of CAS (2010). He also received the Fu Chengyi Youth Science and Technology Award, in 2012, and the Xia Jianbai Award of Geomatics, in 2014. He was the President of the International Association of Planetary Sciences (IAPS), from 2013 to 2017, and the International Association of CPGPS, from 2016 to 2017, the Chair of the IUGG Union Commission on Planetary Sciences (UCPS), from 2015 to 2019, and the Vice-President of the IAG Commission 2, from 2015 to 2019, and the COSPAR's Panel on Satellite Dynamics (PSD) (2016–2020). He has been the Editor-in-Chief of the *International Journal of Geosciences*, since 2010, and an Associate Editor of the IEEE TRANSACTIONS ON GEOSCIENCE AND REMOTE SENSING, since 2014, and *The Journal of Navigation*, since 2014. He was an Associate Editor of *Advances in Space Research*, from 2013 to 2017.

PENGGEN CHENG was born in Nanchang, Jiangxi, China, in 1964. He received the B.S. degree in surveying engineering from the East China Institute of Geology, Fuzhou, Jiangxi, China, in 1985, the M.S. degree in photogrammetry and remote sensing from the Wuhan Technology University of Surveying and Mapping, Wuhan, Hubei, China, in 1996, and the Ph.D. degree in photogrammetry and remote sensing from Wuhan University, Wuhan, in 2005.

He was a Visiting Scholar with the University of Waterloo, Canada, from 2008 to 2009. From 1985 to 2000, he was a Lecturer and an Associate Professor with the Surveying Department, East China Institute of Geology. Since 2000, he has been a Professor with the Faculty of Geomatics, East China University of Technology. He is the author of four books and more than 180 articles. His research interests include geographic information system theory and software development, three-dimensional data model theory and application, remote sensing geo-mapping, and urban ecological environment monitoring.

Dr. Cheng was a recipient of the Yexue'an Excellent Teacher Award, in 2017. He was named a Young and Middle-Aged Expert with outstanding contributions from the National Nuclear Industry Corporation of China, in 1998, and an Expert on special government allowances under the State Council, in 2002. He is also an Editor of *Geography* and *Geographical Information Science*.

YAO YEVENYO ZIGGAH was born in Agona, Ghana, in 1984. He received the B.Sc. degree (Hons.) in geomatics engineering from the Kwame Nkrumah University of Science and Technology (KNUST), Kumasi, Ghana, in 2008, and the M.E. and Ph.D. degrees in geodesy and survey engineering from the China University of Geosciences (CUG), Wuhan, China, in 2013 and 2017, respectively.

Since 2017, he has been a Lecturer with the Geomatic Engineering Department, University of Mines and Technology (UMaT), Ghana. He is the author of more than 48 peer-reviewed journal articles. His research interests include application of artificial intelligence in engineering, 2D/3D coordinate transformation, height systems, gravity field modeling, and geodetic deformation modeling.

Dr. Ziggah was a recipient of the UMaT Staff Development Fund, the Ghana Government Scholarship, and the Chinese Government Scholarship to pursue master's and doctorate degrees. He received the Second Best Paper at the Geographic Information System, Geodesy and Survey Engineering Conference, Changsha, China, in 2015.

LEYANG WANG was born in Linyi, Shandong, China, in 1983. He received the B.S. degree in surveying engineering from the East China University of Technology, Fuzhou, Jiangxi, China, in 2005, the M.S. degree in geodesy and survey engineering from Central South University, Changsha, Hunan, China, in 2008, and the Ph.D. degree in geodesy and survey engineering from Wuhan University, Wuhan, Hubei, China, in 2011.

From 2011 to 2014, he was a Lecturer, and since 2014, he has been an Associate Professor with the Faculty of Geomatics, East China University of Technology. He is the author of more than 80 articles. His research interests include geodetic inversion and surveying adjustment.

Dr. Wang is also an Editorial Board Member of the journal *Jiangxi Cehui*. He has been a Young Jinggang Scholar, since 2018. He was a recipient of the Jiangxi Science Fund for Distinguished Young Scholars, in 2016.

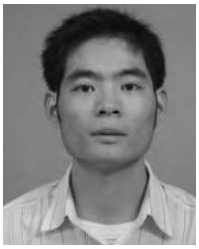

YUQIAN WANG was born in Ezhou, Hubei, China, in 1983. He received the B.S. degree in mathematics from Wuhan University, Wuhan, Hubei, in 2005, the master's degree in mathematics from The Chinese University of Hong Kong, Hong Kong, in 2007, and the Ph.D. degree in photogrammetry and remote sensing from Wuhan University, in 2015. He is currently a Lecturer with the Faculty of Geomatics, East China University of Technology. He has published around 20 papers in various journals and conferences. His research interests include remote sensing data process and applications in resource and environment.

HAIYING HU was born in Yichun, Jiangxi, China, in 1996. She received the B.S. degree in remote sensing science and technology from the East China University of Technology, Nanchang, Jiangxi, in 2018, where she is currently pursuing the master's degree in surveying and mapping. Her research interest includes LiDAR point clouds processing.

YOUJIAN HU was born in Hunan, China, in 1960. He received the B.S. degree in surveying from Henan Polytechnic University, Jiaozuo, Henan, China, in 1982, the M.S. degree in engineering surveying from the PLA Institute of Surveying and Mapping, Zhengzhou, Henan, in 1995, and the Ph.D. degree in geological engineering from the China University of Geosciences, Wuhan, Hubei, China, in 2005.

He was a Visiting Scholar with RMIT University, Australia, from 2013 to 2014. From 1983 to 1992, he was a Lecturer with the Surveying Department, Henan Polytechnic University. From 1993 to 1998, he was an Associate Professor with the Surveying Department, Henan Polytechnic University. Since 1999, he has been a Professor with the Faculty of Information Engineering, China University of Geosciences. He is the author of three books and more than 80 articles. His research interests include engineering deformation and geological hazard monitoring, GNSS data processing, and LiDAR data processing and applications.